Simultaneous electrochemical detection of azithromycin and hydroxychloroquine based on VS$_2$ QDs embedded N, S @graphene aerogel/cCNTs 3D nanostructure

H. Mater Mahnashi [a], Ashraf M. Mahmoud [a,b], A. Saad Alkahtani [c], Mohamed M. El-Wekil [b,*]

[a] *Department of Pharmaceutical Chemistry, College of Pharmacy, Najran University, Najran, Saudi Arabia*
[b] *Department of Pharmaceutical Analytical Chemistry, Faculty of Pharmacy, Assiut University, Assiut, Egypt*
[c] *Department of Clinical Pharmacy, College of Pharmacy, Najran University, Najran, Saudi Arabia*

A B S T R A C T

In this research paper, an innovative electrochemical sensor was suggested for simultaneous voltammetric analysis of azithromycin (AZM) and hydroxychloroquine (HCQ) for the first time. The sensor based on hydrothermal synthesis of vanadium disulfide quantum dots (VS$_2$ QDs) and insertion within 3D N, S graphene aerogel (3D N, S @ GNA) and carbon nanotubes nanaostructure as a new and widely group of carbon nanomaterials. The nanocomposites were characterized morphologically using different techniques. In addition, the nanomaterials were characterized electrochemically using cyclic voltammetry (CV), electrochemical impedance spectroscopy (EIS) and differential pulse voltammetry (DPV). The proposed electrochemical sensor showed wide dynamic linear ranges of $0.28-30 \times 10^{-8}$ M and $0.84-22.5 \times 10^{-8}$ M for analysis of AZM and HCQ, respectively. The limits of detection (LODs) based on signal to noise (S/N) 3:1 were found to be 0.091×10^{-8} M and 0.277×10^{-8} M for AZM and HCQ, respectively. Briefly, the electrochemical sensor had good stability, selectivity, reproducibility and feasibility for simultaneous detection of AZM and HCQ in presence of different interfering species.

1. Introduction

Coronavirus disease (COVID-19) has been labeled as a pandemic by the World Health Organization (WHO) on March 11, 2020 [1]. Some articles are available with the evidence of successful treatment of varying degree. Yet, universally accepted treatment does not exist for this rapidly spreading disease [2]. Some studies have used chloroquine (CQN) or hydroxychloroquine (HCQ) as possible treatments [3,4]. An early study was conducted on Chinese patients, which confirms that CQN, as anti-malarial drug, had a significant effect in terms of viral clearance and clinical outcomes, if compared to controlled group [5,6]. Chinese experts recommend that patients diagnosed as mild, moderate and severe cases of COVID-19 pneumonia and without contraindications to CQN be treated with 500 mg CQN twice a day for ten days [7]. Although AZM is an antibiotic from the macrolide group, it was recorded to have antiviral [8–10] and anti-inflammatory effects [11–13]. The reason behind the significantly improved viral clearance when AZM is added to HCQ can purely be due to the action of AZM. Hence, AZM alone may be fit enough to clear the virus at the initial stage of the disease.

AZM may down regulate inflammatory responses and reduce the excessive cytokine production associated with respiratory viral infections. Gautret et al. and his group describe a trial where HCQ combined with AZM which gives a 100% viral clearance in 6 days [14]. Both HQC/CQN and AZM [15–18] are known to prolong QTc-Interval. The combination can, therefore, cause cardiac side-effects.

In order to obtain clinically trusted data from therapeutic drug monitoring (TDM), we should use highly sensitive and selective analytical methods capable of using small sample volumes, with no interferences from endogenous or exogenous compounds [19].

Recently, electrochemical sensors with an excellent ability for determination of the electro-active substances have been suggested as powerful analytical tool in recent years. Electrochemical sensors are fast, portable and relatively cheap. Different types of conductive and non-conductive mediators such as organic ligands, inorganic complexes, ionic liquid, conductive polymers, nanoparticle and nanocomposite were suggested for the fabrication of selective and powerful electrochemical sensors from many years ago [20–25].

Few electrochemical methods were reported for analysis of HCQ

[26–29] and AZM [30–33]. Some of the reported methods need high cost electrodes (diamond electrode) and/or several fabrication steps (molecular imprinted electrodes). Therefore, the aim of this work is to develop a simple, rapid, cost-effective and sensitive electrochemical sensor for simultaneous voltammetric analysis of HCQ and AZM for the first time.

Quantum dots (QDs) have attracted more attentions as a novel class of nanostructures in many fields. Amongst these QDs, vanadium disulfide quantum dots (VS_2 QDs) is an ideal candidate due to ease of doping, good solubility, and facile functionalization [34,35].

Graphene aerogel (GNA) is a porous 3D nanomaterial with large number of internally crosslinked 3D hollow meshes, which will improve the stability, enhance the conductivity, and adapt to huge volume varies [36].

In view of effective surface area, high stability, superior electronic conductivity and mechanical properties, nanoparticles-embedded graphene and carbon nanotubes (CNTs) hybrid nanostructures are currently attracting wide attention as composite materials to modify electrodes for detection of various analytes [37–39].

In this research paper, a simple, rapid, cost-effective and sensitive electrochemical sensor was proposed for simultaneous analysis of HCQ and AZM. The sensor based on modification of GCE with vanadium disulfide quantum dots decorated nitrogen and sulfur co-doped graphene aerogel/carboxylated carbon nanotubes (VS_2 QDs/N, S@ GNA/cCNTs/ GCE). The proposed sensor showed wide dynamic linear ranges and low detection limits. The proposed sensor presented good reproducibility, feasibility and selectivity for simultaneous detection of AZM and HCQ in different matrices.

2. Experimental

2.1. Materials and reagents

Azithromycin ($\geq$98%) was obtained as a gift from NODCAR, Giza, Egypt. Hydroxychloroquine sulfate ($\geq$98%), graphene oxide, ammonium vanadate ($\geq$99%), uric acid ($\geq$99%), methionine ($\geq$99%), cysteine ($\geq$97%), adenine ($\geq$98%), guanine ($\geq$98%), glutathione (($\geq$99%) and carbon nanotubes (CNTs) were purchased from Sigma Aldrich. 2-Aminobenzothiazole (2-ABTHZ) ($\geq$98%), dopamine HCl ($\geq$98%) and glucose ($\geq$97%) were purchased from Merck. Potassium permanganate, ascorbic acid, sodium nitrate, hydrochloric acid (37%), ferrocyanide, ferricyanide, boric acid, phosphoric acid (85%) and acetic acid ($\geq$97%) were purchased from El-Nasr for intermediate chemicals, Cairo, Egypt. Double distilled water (DDW) was used along the whole study. Zithromax® capsules (500 mg AZM) and hydroquine® tablets (200 mg HCQ) were obtained from local markets.

2.2. Instrumentation

Descriptions of instruments used for analysis and characterization of nanomaterials were included within the electronic supplementary materials (ESM).

2.3. Preparation of vanadium disulfide quantum dots (VS_2 QDs)

Vanadium disulfide quantum dots can be prepared via hydrothermal method. Ammonium vanadate (0.05 mM) was mixed with cysteine (0.03 mM) in double distilled water, and stirring until complete dissolution. The mixture was heated at 180 °C for 10 h prior to cooling to room temperature. The obtained solution was centrifuged at 4000 rpm for 15 min and then, the supernatant was filtered using 0.22 μm filter paper.

2.4. Preparation of 3D nitrogen and sulfur co-doped graphene aerogel (3D N, S @ GNA)

Graphene oxide (50 mg) and 100 mg 2-ABTHZ were mixed with 150 mL double distilled water to form homogenous dispersion. The suspension was heated at 180 °C for 8 h before cooling to room temperature. The product was washed 5 times with ethanol and double distilled water, and then freeze dried.

2.5. Preparation of VS_2 QDs/cCNTs/3D N, S@GNA/GCE

N, S@ GNA and cCNTs (200 mg for each) were suspended in 10 mL ethanol by sonication for 20 min. Then, 100 mg of VS_2 QDs was added to the previous suspension and sonication was maintained for 30 min. The resultant suspension was used to modify GCE by drop casting 5 μL of VS_2 QDs/cCNTs/N, S@GNA dispersion. Scheme 1 describes the main steps for preparation of VS_2 QDs/cCNTs/N, S@GNA/GCE and its utility for electro-oxidation of AZM and HCQ.

2.6. Preparation of real samples

Urine samples were collected from healthy volunteers and 5 mL of urine sample was centrifuged at 1500 rpm for 20 min. Then, the urine sample was filtered using 0.45 mm filter paper and 1.5 mL of the supernatant was transferred to voltammetric sample containing B.R. buffer (pH = 6.0).

Human plasma (1.5 mL) was mixed with 1.0 mL acetonitrile and subjected to centrifugation to about 30 min to remove possible interference. After that, the supernatant was collected and diluted with 5 mL B.R. buffer (pH = 6.0) prior to the voltammetric analysis.

Twenty tablets or the contents of 20 capsules of each dosage form were weighed, and then finely powdered using mortar and pestle. Equivalent amounts of the powder to one tablet or capsule were weighed accurately The weighed powders were dissolved in a 20 mL methanol and sonicated for 10 min to ensure complete solubility and filtered. Then, the filtrate was transferred into a 100 mL standard flask and diluted to the final volume with methanol, and then subjected to our procedure.

3. Results and discussions

3.1. Characterization of VS_2 QDs

TEM, FTIR and UV–Vis techniques were used to demonstrate of the synthesized VS_2 QDs by heating with ammonium vanadate and cysteine (Fig. 1a-c). Fig. 1a shows the TEM image of VS_2 QDs with average size of that ~9.2 nm (Fig. 1d). The FTIR spectrum was used to characterize the VS_2 QDs and refer to the most important functional groups (Fig. 1b). The presence of bands at 3345 cm^{-1}, 1670 cm^{-1}, 1665 cm^{-1} and 1350 cm^{-1} corresponding to ν (OH), δ (OH), ν (C=O) and ν (C-NH-C), respectively confirm the good formation of VS_2 QDs. Moreover, the characteristic bands of VS_2 QDs are the ν (V=S) and ν (V-S-V) that locates at 1070 cm^{-1} and 590–670 cm^{-1}, respectively. The optical properties of quantum dots with UV–Vis and fluorescence spectroscopy were examined. The UV–Vis spectrum was obtained in aqueous solution with the appearance of two bands at 230 nm and 345 nm which correspond to π-π* and n-π* transitions [40,41]. The fluorescence spectrum of VS_2 QDs was presented in Fig. 1c where it shows emission at 445 nm after the excitation at 370 nm.

3.2. Morphological characterization of 3D N, S@GNA, 3D N, S@GNA/ cCNTs and VS_2 QDs/3D N, S@ GNA/cCNTs

SEM, TEM, FTIR, Raman spectroscopy and PXRD techniques were used to characterize the synthesized nanomaterials. As shown in Fig. S1a, the SEM images of cCNTs show high surface area, good dispersion and tubular like shapes while Fig. S1b exhibits thin layer of N,
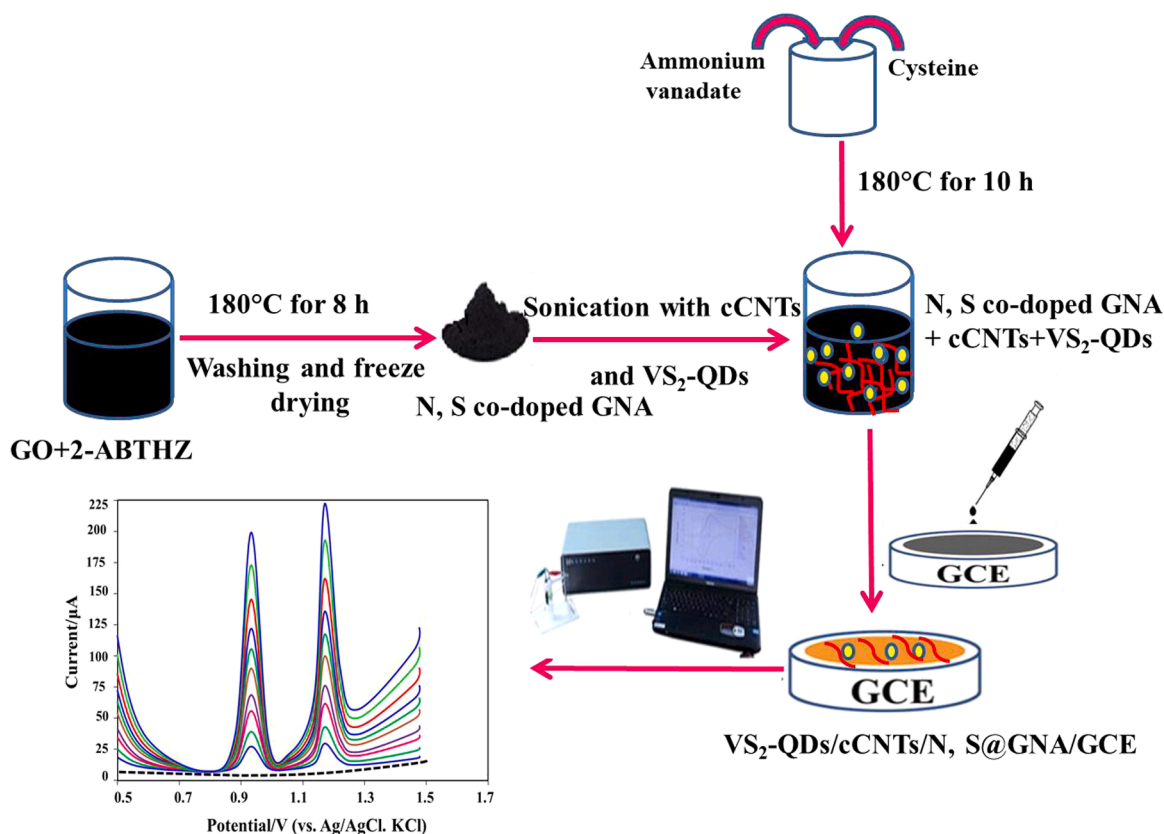
Scheme 1. Main steps for preparation of VS$_2$ QDs/cCNTs/N, S@GNA/GCE and its role for electro-oxidation of AZM and HCQ.

S@GNA. Fig. S1c shows good dispersion of VS$_2$ QDs and cCNTs on N, S@GNA, which is confirmed by TEM image in Fig. S1d.

FTIR spectra of N, S@GNA, cCNTs and VS$_2$ QDs/N, S@ GNA/cCNTs were presented in Fig. S2. It is seen from Fig. S2a that the characteristic bands of N, S-GNA exhibit the ν (OH) at 3380 cm^{-1}, ν (C=O) at 1715 cm^{-1}, ν (C=C) at 1652 cm^{-1} and ν (C-S, C-N) at 1240 cm^{-1}. The FTIR bands of N, S-GNA/cCNTs are seen in Fig. S2b at 3385 cm^{-1}, 2840–2930 cm^{-1}, 1715 cm^{-1}, 1652 cm^{-1} and 1240 cm^{-1} which are assigned to ν (OH), ν (CH), ν (C=O), ν (C=C) and ν (C-S, C-N), respectively. Fig.S2c shows the FTIR bands of VS$_2$ QDs/N, S@ GNA/cCNTs that exhibits the ν (V=S) at 1050 cm^{-1} and ν (V-S) at 530–620 cm^{-1}.

The EDS was carried out to show the elements contents of nano-composite. The presence of S, V, C and O elements in EDS show successful combination of VS$_2$ QDs/N, S@ GNA/cCNTs (Fig. S3).

The PXRD patterns of VS$_2$ QDs and VS$_2$ QDs/N, S@ GNA/cCNTs are presented in Fig. S4. The diffraction peaks that correspond to (0 0 1), (1 0 0), (0 1 1), (0 1 2), (1 1 0), (1 0 3), (0 0 4) of VS$_2$ QDs are present at 15.54°, 33.32°, 36.32°, 44.34°, 56.34°, 58.84° and 66.23°, respectively [42,43]. Besides all the peaks of VS$_2$ QDs, the peak at approximately 26° corresponds to the N, S@GNA/cCNTs nanocomposite [44].

Raman spectroscopy was studied to confirm the successful formation of nanostructure. Fig. S5 shows the Raman bands of VS$_2$ QDs at 470 cm^{-1} and 580 cm^{-1} that corresponds to the in-plane vibration E$^1_{2g}$ mode and the out-plane vibration mode (A1g), respectively. In addition, the presence of D and G bands of N, S@GNA/cCNTs are observed at 1350 cm^{-1} and 1580 cm^{-1}, respectively.

3.3. Electrochemical characterization of 3D N, S@GNA, 3D N, S@GNA/cCNTs and VS$_2$ QDs/3D N, S@ GNA/cCNTs

The electrochemical surface area was calculated from the voltammetric peak current by use of the Randle-Sevcik equation:

$$Ipa = 2.69 \times 10^5 AD^{1/2}n^{3/2}v^{1/2}C$$

where Ipa is the anodic peak current. A is the surface area. n is the number of electron involved in redox reaction (n = 1). D is the diffusion coefficient of the molecule in solution (7.6 $\times$ 10^{-6} cm^2 s^{-1}). C is the concentration of the probe molecule (5 mM [Fe(CN)$_6$]$^{3-/4-}$). v is the scan rate. From the slope of the Ipc - v$^{1/2}$ relationship, the surface areas of bare GCE, 3D N, S@GNA/GCE, 3D N, S@GNA/cCNTs/GCE and VS$_2$ QDs/3D N, S@ GNA/cCNTs/GCE were calculated to be 0.391, 0.541, 1.393 and 2.652 cm^2 (Fig. S6).

Moreover, electrochemical impedance spectroscopy (EIS) was used to investigate the surface properties of the modified sensor [45]. The semicircle part in Nyquist plots equals to the electron transfer resistance (Rct). Fig. S7 shows the EIS of bare GCE, 3D N, S@GNA/GCE, 3D N, S@GNA/cCNTs/GCE and VS$_2$ QDs/3D N, S@ GNA/cCNTs/GCE. It is obvious that large semicircle is found at bare GCE, which is decreased upon modifications with nanomaterials. This phenomenon proves that successive modification with 3D N, S@GNA, cCNTs and VS$_2$ QDs improves the conductivity and electron transfer properties of the electrode.

3.4. Electrochemical performance at various electrodes

The electrochemical behaviors of 20.0 μM of AZM and HCQ on bare GCE (a),3D N, S@GNA/GCE (b), 3D N, S@GNA/cCNTs/GCE (c) and VS$_2$ QDs/3D N, S@ GNA/cCNTs/GCE (d) were investigated by CV in B.R. buffer (pH 6.0) (Fig. S8). As shown, there is no redox peaks at the bare GCE, which is due to the slow electron transfer. In comparison, well-defined oxidation peaks of AZM and HCQ were obtained at 3D N, S@GNA/GCE owing to the good conductivity of 3D N, S@GNA. For 3D N, S@GNA/cCNTs/GCE, a larger redox peaks currents were observed as a result of increasing the conductivity and surface area by cCNTs. More interestingly, VS$_2$ QDs/3D N, S@ GNA/cCNTs/GCE shows much higher
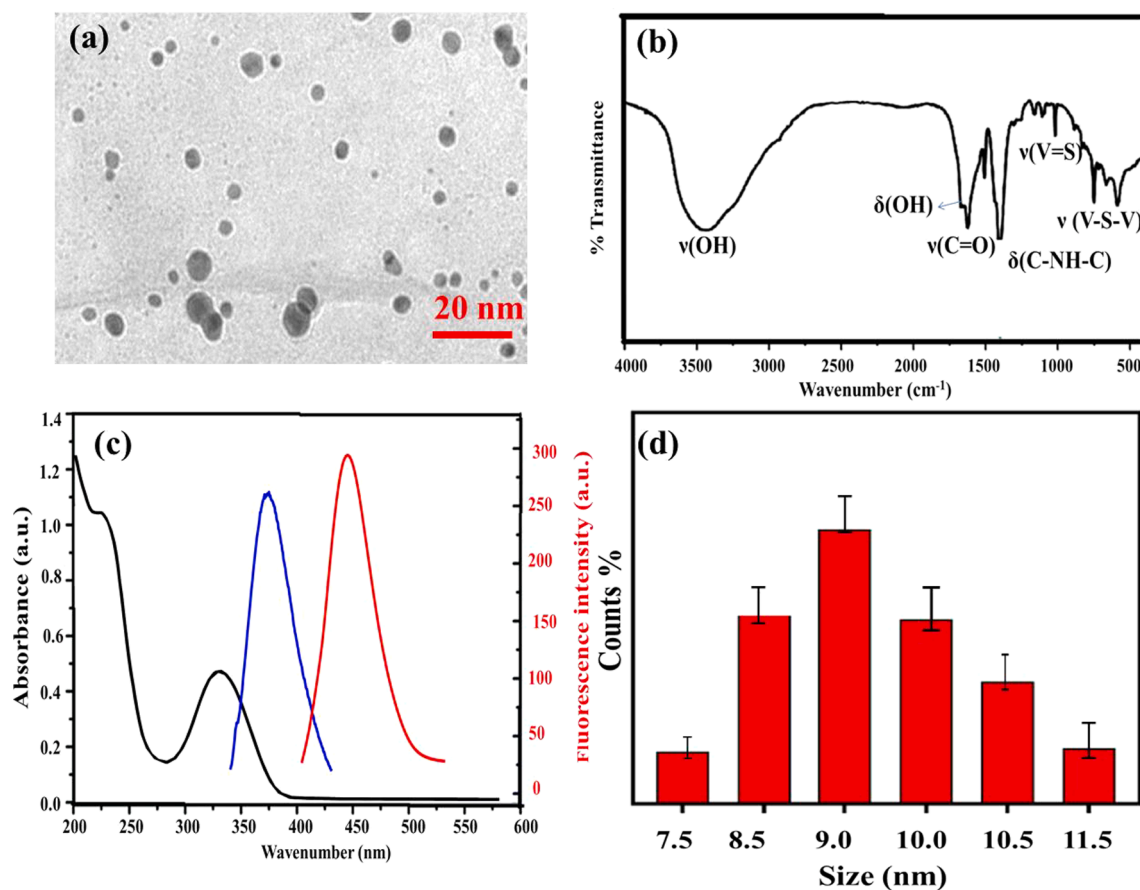
Fig 1. (a) TEM, (b) FTIR, (c) Absorbance/fluorescence spectra and (d) size distribution of VS$_2$ QDs.

oxidation peaks' currents. The excellent performance accounts for the synergistic effects of VS$_2$ QDs/ 3D N, S@ GNA/cCNTs, including the high adsorption capacity, enhanced electron transfer, as well as the increased catalytic active sites on the electrode.

3.5. Optimization of DPV variables

Effect of pH on the electrochemical behavior of 12.5×10^{-8} M at VS$_2$ QDs/3D N, S@ GNA/cCNTs/GCE in B.R. buffer (pH 6.0) was investigated by DPV at a pH range of 4.0~8.0 (Fig.S9A). As observed from Fig. S9B, the anodic peak current of AZM and HCQ achieved a maximum value at pH of 6.0, which was chosen for subsequent current measurements.

Besides, with the enhancing pH, the anodic peak currents (Ipa) shifted towards more negative values, suggesting that protons took part in the electrochemical reaction. Meanwhile, the oxidation peak potential (Epa) was linearly depended on the pH values of the solution, which obeys the following equation of Epa (V) = 1.208–0.051 pH (R^2 = 0.996) and Epa (V) = 1.528–0.057 pH (R^2 = 0.993) for AZM and HCQ, respectively (Fig. S9C). The slope of −52 mV pH^{-1} was close to the theoretical slope of −59 mV pH^{-1}, illustrating that the number of protons and electrons occurred in the electro-oxidation process of AZM and HCQ is equal [46–48].

The adsorption capacity of AZM and HCQ can be obviously improved by preconcentration step. Therefore, the influence of preconcentration time and potential were optimized. From Fig.S10A, it can be seen that the oxidation current gradually increased with increasing preconcentration time from 20 to 300 s. This is because that more molecules were adsorbed onto the electrode surface. However, the peak current changed slightly as further increasing accumulation time from 200 to 300 s, suggesting that the amount of AZM and HCQ at the VS$_2$ QDs/N, S@

GNA/cCNTs/GCE tended to a limiting value. Thus, 200 s was employed as the optimal preconcentration time.

The optimum preconcentration potential was investigated in the range from +0.1 V to 0.8 V (Fig. S10B). The peak current increased with increasing the potential from −0.2 to 0.5 V. However, the response current decreased when the potential was over 0.5 V. Consequently, preconcentration potential of 0.5 V was selected in the following further experiments.

3.6. Effect of potential scan rate

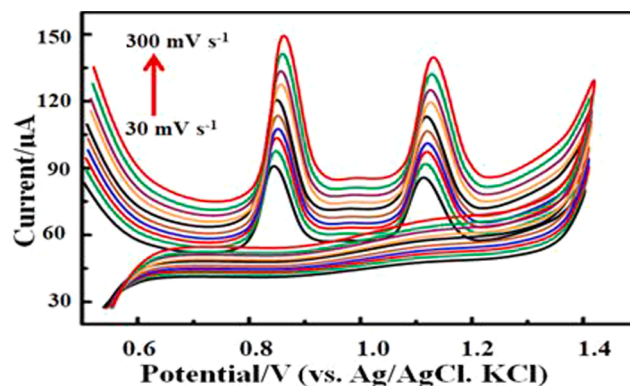The effect of scan rate on the electro-oxidation of AZM and HCQ at

Fig 2. (A) CV scans of 15.0 µM of AZM and HCQ at VS$_2$ QDs/3D N, S@ GNA/cCNTs/GCE in B.R. buffer (pH 6.0) at scan rate of 200 mv s^{-1} after preconcentration time of 150 s.

VS_2 QDs/3D N, S@ GNA/cCNTs/GCE in B.R. buffer (pH 6.0) was investigated in the range of 30–300 mV s^{-1} (Fig. 2). Upon increasing the potential scan rate, the anodic peak currents (Ipa) was increased with shift the oxidation potential to more positive values. The relationship between log Ipc (μA) and log ν (mV s^{-1}) can be expressed by the following equations: Ipa (μA) = 0.218 log ν (mVs^{-1}) + 87.47 (R^2 = 0.9951) and Ipa (μA) = 0.211 log ν (mVs^{-1}) + 80.07 (R^2 = 0.9959) for AZM and HCQ, respectively [49,50].

The number of electrons involved within the oxidation of AZM and HCQ was calculated using the following formula for irreversible reactions [51]: $an = 0.048/Ep - Ep/2$

Where α is charge transfer coefficient, Ep/2 is potential at half peak current and n is the number of electrons consumed in the electrochemical oxidation. The obtained Ep/2 for oxidation of AZM and HCQ at the VS_2 QDs/3D N, S@ GNA/cCNTs/GCE in B.R. buffer (pH 6.0) was found to be 1.03. Thus, the number of electrons consumed in the oxidation process, assuming α for irreversible reactions = 0.5, was found to be 1.96 and 2.03 for AZM and HCQ, respectively (≈two electrons for each) (Scheme 2).

3.7. Stability and reproducibility of VS_2 QDs/3D N, S@ GNA/cCNTs/GCE

The stability of VS_2 QDs/3D N, S@ GNA/cCNTs/GCE was evaluated by storing the modified sensor at room temperature and used for detection of 15.0 μM of AZM and HCQ in B.R. solution (pH 6.0) by CV as shown in Fig. S11A. The graph displayed in the inset of Fig. S11A shows the CV response which indicates good stability as the decrease in

oxidation peak currents of the fabricated sensor was about 4.7% after four weeks of storage. The reproducibility of VS_2 QDs/3D N, S@ cCNTs/GCE was investigated after incubation of eight modified electrodes, following a similar fabrication conditions for detection of 15.0 μM of AZM and HCQ in B.R. solution (pH 6.0) by CV as shown in Fig. S11B. The diagram displayed in the inset of Fig. S11B demonstrates the good reproducibility with RSD % less than 3.6%.

3.8. DPV analysis of AZM and HCQ in standard solutions, human serum and urine samples

The electrochemical analysis of AZM and HCQ using VS_2 QDs/3D N, S@ GNA/cCNTs/GCE was conducted using DPV. The anodic peaks are sharper and better defined at lower concentrations of the two drugs. Fig. 3 shows DPV scans obtained in pure forms in the concentration ranges of 0.28–30 × 10^{-8} M and 0.84–22.5 × 10^{-8} M for AZM and HCQ, respectively under optimized conditions of pulse height, pulse width, step height and preconcentration time of 40 mV, 0.08 s, 15 mV and 200 s respectively. The anodic peak currents (Ipa) increases linearly with the increase of AZM and HCQ concentrations. The regression equations of AZM and HCQ are Ipa = 6.53C + 4.72 (R^2 = 9989) and Ipa = 8.93C + 16.599 (R^2 = 0.9993) with LODs of 0.09 and 0.28 × 10^{-8} M, respectively (Table 1). The intra-day and inter-day precisions of the proposed voltammetric method were investigated and presented in Table S1.

3.9. Selectivity

Selectivity of the proposed VS_2 QDs/3D N, S@ GNA/cCNTs/GCE was
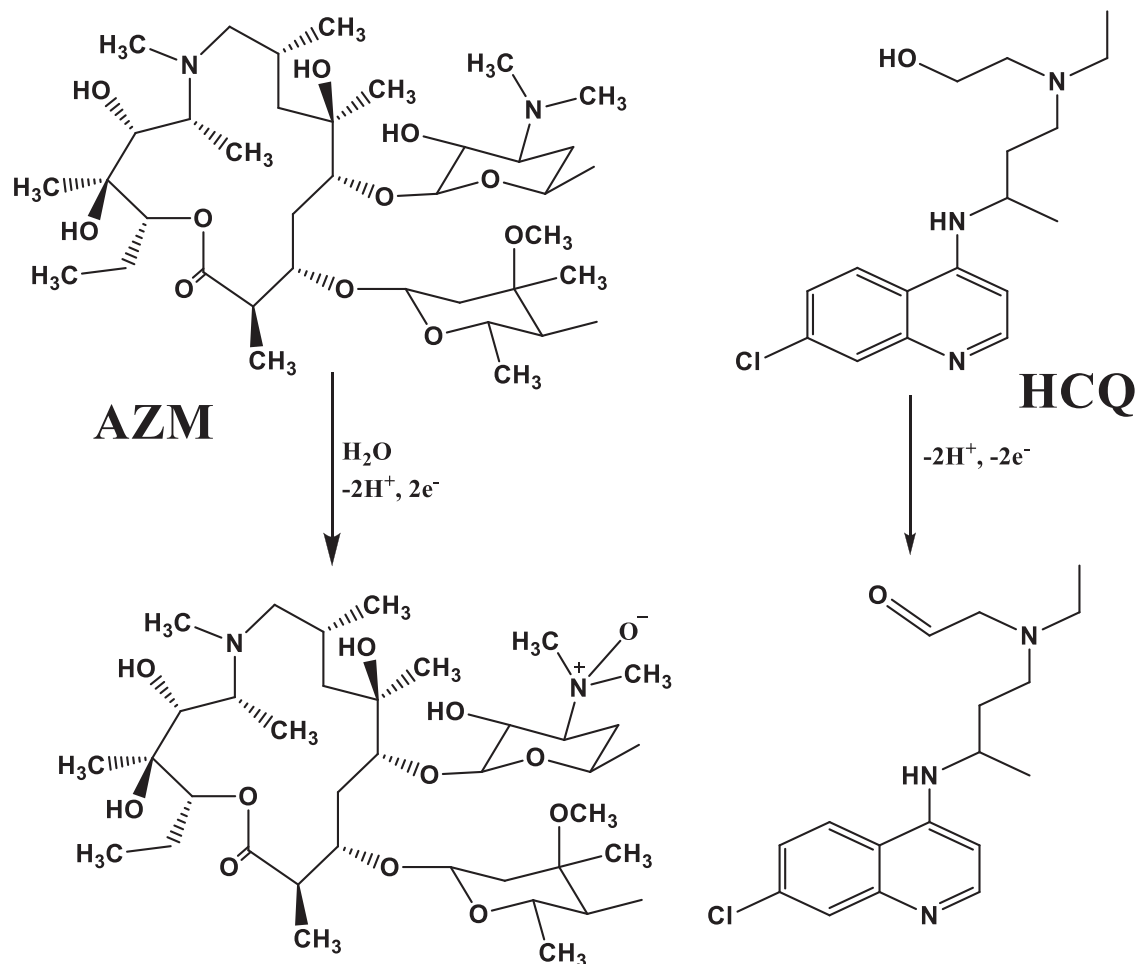
Scheme 2. The electrochemical oxidation of AZM and HCQ at VS_2 QDs/3D N, S@ GNA/cCNTs/GCE in B.R. buffer (pH 6.0).
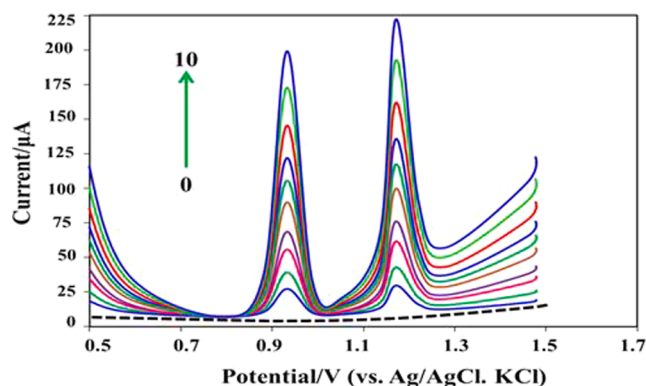
Fig 3. (A) The DPV responses of VS$_2$ QDs/3D N, S@ GNA/cCNTs/GCE for simultaneous detection of AZM and HCQ in B.R. solution (pH 6.0) at different concentrations. (B) Calibration plots of Ipa vs. concentration under the optimum conditions of measurement.

examined in presence of some co-existing interfering substances in presence of 8.5 × 10^{-8} M AZM and HCQ. The results shown in Fig. 4 prove that 500 folds of ascorbic acid, uric acid, methionine, glutathione, glucose and dopamine; 400 folds of adenine and guanine did not affect the anodic currents of AZM and HCQ. The good selectivity of VS2 QDs/ 3D N, S@ GNA/cCNTs towards detection of AZM and HCQ is mainly attributed to the oxidation potentials of AZM and HCQ, and may be attributed to the hydrophobic interactions between the investigated analytes and nanohybrid, facilitating their adsorption onto the electrode surface.

3.10. Robustness

Robustness of analytical method is the ability to resist small change upon variation of some operational parameters such as pH, preconcentration potential and time, and pulse height. The mean percentage recovery (recovery %) and % relative standard deviation (RSD %) values were not significantly affected by these variations (Table S2). Based on these results, the proposed electrode suggested for analysis of AZM and HCQ is reliable for quantification of these drugs with robust results.

3.11. Analytical applications in real samples

The analytical applicability of VS$_2$ QDs/3D N, S@ GNA/cCNTs/GCE was evaluated by detecting of AZM and HCQ in pharmaceutical formulations, human serum and urine samples. Typical DPV scans for successive additions of AZM in human serum and human urine are depicted in Fig. S12. The relationships between anodic peak currents (Ipa) and the added concentrations in pharmaceutical formulations and biological samples are straight lines with satisfactory correlation coefficients. The results for detection of AZM and HCQ by standard addition method are cited in Table 1. The samples were analyzed by HPLC method, and it was found that no significant difference between the proposed and HPLC methods. Consequently, the proposed sensor is accurate for AZM and HCQ assay in human serum and urine samples with high accuracy.

4. Comparison with other reported sensors

AZM and HCQ were individually analyzed by different electrochemical sensors. In comparison, the proposed electrochemical method shows many advantages such as simplicity, rapidity, cost effective and

Table 1
Analysis of AZM and HCQ by VS$_2$ QDs/3D N, S@ GNA/cCNTs/GCE in serum, urine and pharmaceutical formulations (n = 3).

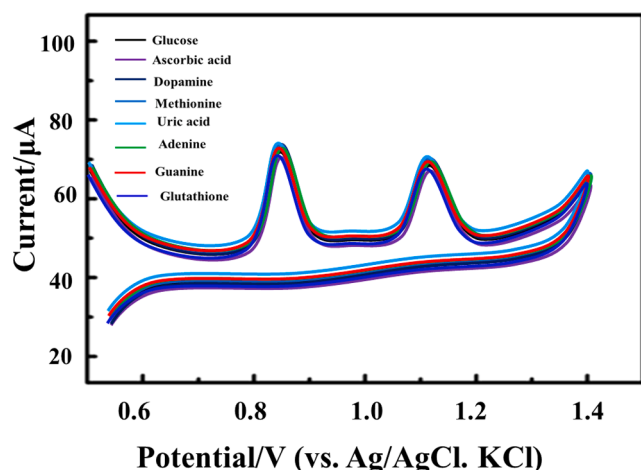| Samples	Added (×10^{-8} M)	Proposed sensor						HPLC method					
		AZM			HCQ			AZM			HCQ		
		Found (×10^{-8} M)	Recovery %±SD	RSD %	Found (×10^{-8} M)	Recovery %±SD	RSD %	Found (×10^{-8} M)	Recovery %±SD	RSD %	Found (×10^{-8} M)	Recovery %±SD	RSD %
Serum 1													
	5.0	4.98	99.6 ± 2.5	2.5	5.05	101.0 ± 2.5	2.4	4.87	97.4 ± 3.2	3.3	5.13	102.6 ± 2.9	2.8
	15	15.34	102.3 ± 3.1	3.1	14.76	98.4 ± 3.3	3.3	15.34	102.3 ± 4.2	4.1	15.32	102.1 ± 3.5	3.4
Serum 2													
	5.0	5.08	101.6 ± 2.9	2.9	4.97	99.4 ± 1.9	1.9	4.87	97.4 ± 2.6	2.7	4.92	98.4 ± 4.1	4.2
	15.0	14.78	98.5 ± 3.7	3.7	15.12	100.8 ± 2.1	2.1	14.56	97.1 ± 3.8	3.9	14.76	98.4 ± 3.8	3.8
Urine 1													
	10.0	9.87	98.7 ± 2.9	3.0	10.25	102.5 ± 2.1	2.1	10.25	102.5 ± 2.5	2.5	9.56	95.6 ± 2.3	2.5
	20.0	19.45	97.3 ± 3.2	3.3	20.34	101.7 ± 3.0	3.0	20.67	103.4 ± 3.1	3.0	19.23	96.2 ± 3.6	3.7
Urine 2													
	10.0	10.23	102.3 ± 2.8	2.7	10.27	102.7 ± 3.0	3.0	9.57	95.7 ± 3.8	4.0	10.47	104.7 ± 3.1	2.9
	20.0	20.89	104.5 ± 1.9	1.8	19.65	98.3 ± 2.1	2.2	19.45	97.3 ± 4.0	4.1	20.35	101.8 ± 2.5	2.4
Zithromax® capsules													
	10.0	9.78	97.8 ± 2.7	2.8	–	–	–	9.57	95.7 ± 2.8	2.9	–	–	–
	20.0	19.34	96.7 ± 3.1	3.2	–	–	–	19.45	97.3 ± 3.5	3.6	–	–	–
Hydroquine® tablets													
	10.0	–	–	–	9.67	96.7 ± 3.1	3.2	–	–-	–	10.12	101.2 ± 2.4	2.4
	20.0	–	–	–	20.67	103.4 ± 2.8	2.7	–	–-	–	19.78	98.5 ± 3.6	3.7

Fig 4. DPV scans of VS$_2$ QDs/3D N, S@ GNA/cCNTs/GCE in measuring of 10.0 μM of AZM and HCQ in presence of different interfering species.

low values of LODs (Table S3).

5. Conclusions

This paper describes a novel combination for simultaneous electrochemical sensing of AZM and HCQ as a possible treatment of COVID-19 overloads. The sensor based on modification of glassy carbon electrode surface with VS$_2$ QDs/3D N, S@ GNA/cCNTs nanohybrid. The VS$_2$ QDs nested in the N, S@ GNA/cCNTs offered more catalytically active sites, while the N, S@ GNA and cCNTs acted as a conductive substrate to fix and sputter VS$_2$ QDs to avert the agglomeration of VS$_2$ QDs and facilitate the electron transfer. The electrode showed an excellent electro-catalytic activities and acceptable electron transfer. In addition, it exhibited wide linear ranges and lower detection limits for analysis of AZM and HCQ than other reported methods. The electrochemical sensor was applied for analysis of AZM and HCQ in human plasma and urine samples as well as pharmaceutical dosage forms. The sensor showed good stability, reproducibility and selectivity. This work may provide a new way for development electro-catalyst based on the combination of VS$_2$ QDs, cCNTs and N, S-GNA.

CRediT authorship contribution statement

H. Mater Mahnashi: Resources, Writing - review & editing, Funding acquisition. **Ashraf M. Mahmoud:** Investigation, Software, Validation, Visualization, Writing - review & editing. **A. Saad Alkahtani:** Funding acquisition, Project administration, Resources, Writing - review & editing. **Mohamed M. El-Wekil:** Conceptualization, Data curation, Formal analysis, Investigation, Methodology, Software, Supervision, Validation, Visualization, Writing - original draft, Writing - review & editing.

Declaration of Competing Interest

The authors declare that they have no known competing financial interests or personal relationships that could have appeared to influence the work reported in this paper.

Acknowledgements

Appendix A. Supplementary data

Supplementary data to this article can be found online at https://doi.org/10.1016/j.microc.2021.105925.

References

[1] M.V. Domenico Cucinotta, WHO Declares COVID-19 a Pandemic, Acta Biomed. 91 (2020) 157–160.

[2] S. H. J. G. Liying Dong, Discovering Drugs to Treat Coronavirus Disease 2019 (COVID-19), Drug Discoveries Therapeutics 12 (2020) 58-60.

[3] J. Gao, Z. Tian, X. Yang, Breakthrough: Chloroquine phosphate has shown apparent efficacy in treatment of COVID-19 associated pneumonia in clinical studies, Biosci. Trends 14 (2020) 72–73.

[4] A. Cortegiani, G. Ingoglia, M. Ippolito, A. Giarratano, S. Einav, A systematic review on the efficacy and safety of chloroquine for the treatment of COVID-19, J. Crit. Car. (2020).

[5] J. Gao, Z. Tian, X. Yang, Breakthrough: Chloroquine phosphate has shown apparent efficacy in treatment of COVID-19 associated pneumonia in clinical studies, Biosci. Trends (2020).

[6] Chinese Clinical Trial Registry. http://www.chictr.org.cn/ searchproj.aspx?.

[7] A. Elavarasi, M. Prasad, T. Seth, R.K. Sahoo, K. Madan, N. Nischal, M. Soneja, A. Sharma, S.K. Maulik, Shalimar, P. Garg, Chloroquine and hydroxychloroquine for the treatment of COVID-19: a systematic review and meta-analysis, J. Gen. Intern. Med. 35 (2020) 3308–3314.

[8] M. Menzel, H. Akbarshahi, L. Bjermer, L. Uller, Azithromycin induces anti-viral effects in cultured bronchial epithelial cells from COPD patients, Sci. Rep. 6 (2016) 28698.

[9] A. Schoegler, B.S. Kopf, R.J. Muster, E. Kieninger, C. Casaulta, A. Jung, A. Moeller, T. Geiser, N. Regamey, M.P. Alves, Antiviral activity of azithromycin in cystic fibrosis airway epithelial cells, J. Europ. Resp. 44 (2014) 3450.

[10] M. Iannetta, G. Ippolito, E. Nicastri, Azithromycin shows anti-zika virus activity in human glial cells, Antimicrob. Agents Chemother. 61 (2017) 61.

[11] G.W. Amsden, Anti-inflammatory effects of macrolides—an underappreciated benefit in the treatment of community-acquired respiratory tract infections and chronic inflammatory pulmonary conditions? J. Antimicrob. Chemother. 55 (2005) 10–21.

[12] A. Ianaro, A. Ialenti, P. Maffia, L. Sautebin, L. Rombolà, R. Carnuccio, T. Iuvone, F. D'Acquisto, M.D. Rosa, Anti-inflammatory activity of macrolide antibiotics, J. Pharmacol. Exp. Ther. 292 (2000) 156–163.

[13] A. Beigelman, S.P. Gunsten, C.L. Mikols, I. Vidavsky, C.L. Cannon, S.L. Brody, M. J. Walter, Azithromycin attenuates airway inflammation in a noninfectious mouse model of allergic asthma, Chest 136 (2009) 498–506.

[14] P. Gautret, J. C. Lagier, P. Parola, V. T. Hoang, L. Meddeb, M. Mailhe, B. Doudier, J. Courjon, V. Giordanengo, V. E. Vieira, H. T. Dupont, S. Honor, P. Colson, E. Chabriere, B. Scola, J. Rolain, P. Brouqui, D. Raoult. Hydroxychloroquine and azithromycin as a treatment of COVID-19: results of an open-label non-randomized clinical trial. Int. J. Antimicrob. Agents. 2020, 105949.

[15] M.D.G. Bustos, B. Diquet, P. Thomare, D. Warot, The pharmacokinetics and electrocardiographic effects of chloroquine in healthy subjects, Trop. Med. Parasitol. 45 (1994) 83–86.

[16] S. Pukrittayakamee, J. Tarning, J. Tarning, P. Jittamala, P. Charunwatthana, S. Lawpoolsri, S.J. Lee, S.J. Lee, W. Hanpithakpong, W. Hanpithakpong, B. Hanboonkunupakarn, N.P.J. Day, N.P.J. Day, E.A. Ashley, E.A. Ashley, N. J. White, N.J. White, Pharmacokinetic interactions between primaquine and chloroquine", Antimicrob. Agents Chemother. 58 (2014) 3354–3359.

[17] J.C. Hancox, M. Hasnain, W.V.R. Vieweg, E.L.B. Crouse, A. Baranchuk, Azithromycin, cardiovascular risks, QTc interval prolongation, torsade de pointes, and regulatory issues: a narrative review based on the study of case reports 2013. [Online]. Available: https://ncbi.nlm.nih.gov/pmc/articles/pmc4040726. [Accessed 21 3 2020].

[18] R.A. Lee, A. Guyton, D.F. Kunz, G. Cutter, C.J. Hoesley, Evaluation of baseline corrected QT interval and azithromycin prescriptions in an academic medical center, J. Hospital Med. 11 (2016) 15–20.

[19] M.M. El-Wekil, A.M. Mahmoud, A.A. Marzouk, S.A. Alkahtani, R. Ali, A novel molecularly imprinted sensing platform based on MWCNTs/AuNPs decorated 3D starfish like hollow nickel skeleton as a highly conductive nanocomposite for selective and ultrasensitive analysis of a novel pan-genotypic inhibitor velpatasvir in body fluids, J. Mol. Liq. 271 (2018) 105–111.

[20] H. Karimi-Maleh, C.T. Fakude, N. Mabuba, G.M. Peleyeju, O.A. Arotiba, The determination of 2-phenylphenol in the presence of 4-chlorophenol using nano-Fe$_3$O$_4$/ionic liquid paste electrode as an electrochemical sensor, J. Colloid Interface Sci. 554 (2019) 603–610.

[21] M. Miraki, H. Karimi-Maleh, M.A. Taher, S. Cheraghi, F. Karimi, S. Agarwal, V. Kumar Gupta, Voltammetric amplified platform based on ionic liquid/NiO nanocomposite for determination of benserazide and levodopa, J. Mol. Liquids 278 (2019) 672–676.

[22] H. Karimi-Maleh, F. Karimi, S. Malekmohammadi, N. Zakariae, R. Esmaeili, S. Rostamnia, M.L. Yola, N. Atar, S. Movaghgharnezhad, S. Rajendran, A. Razmjou, Y. Orooji, S. Agarwal, V. Kumar Gupta, An amplified voltammetric sensor based on platinum nanoparticle/polyoxometalate/two-dimensional hexagonal boron nitride nanosheets composite and ionic liquid for determination of N-hydroxysuccinimide in water samples, J. Mol. Liquids 310 (2020) 113185.

[23] F. Tahernejad-Javazmi, M. Shabani-Nooshabadi, H. Karimi-Maleh, 3D reduced graphene oxide/FeNi$_3$-ionic liquid nanocomposite modified sensor; an electrical synergic effect for development of tert-butylhydroquinone and folic acid sensor, Compos. Part B 172 (2019) 666–670.

[24] H. Karimi-Maleh, F. Karimi, Y. Orooji, G. Mansouri, A. Razmjou, A. Aygun, F. Sen, A new nickel-based co-crystal complex electrocatalyst amplified by NiO dope Pt nanostructure hybrid; a highly sensitive approach for determination of cysteamine in the presence of serotonin, Sci. Rep. 10 (2020) 11699.

[25] H. Karimi-Maleh, F. Karimi, M. Alizadeh, A.L. Sanati, Electrochemical sensors, a bright future in the fabrication of portable kits in analytical systems, Chem. Rec. 20 (2020) 682–692.

[26] M.L.P.M. Arguelho, J.F. Andrade, N.R. Stradiotto, Electrochemical study of hydroxychloroquine and its determination in plaquenil by differential pulse voltammetry, J. Pharm. Biom. Anal. 32 (2003) 269–275.

[27] P.B. Deroco, F.C. Vicentini, G.G. Oliveira, R.C. Rocha-Filho, O. Fatibello-Filho, Square-wave voltammetric determination of hydroxychloroquine in pharmaceutical and synthetic urine samples using a cathodically pretreated boron-doped diamond electrode, J. Electroanal. Chem. 719 (2014) 19–23.

[28] A. Khoobi, S.M. Ghoreishi, M. Behpour, M. Shaterian, M.S. Niasari, Design and evaluation of a highly sensitive nanostructure-based surface modification of glassy carbon electrode for electrochemical studies of hydroxychloroquine in the presence of acetaminophen, Colloids Surf. B: Biointerfaces 123 (2014) 648–656.

[29] A. Khoobi, S.M. Ghoreishi, M. Behpour, Sensitive and selective determination of hydroxychloroquine in the presence of uric acid using a new nanostructure self-assembled monolayer modified electrode: optimization by multivariate data analysis, Analyst 139 (2014) 4064–4072.

[30] P. Rebelo, J.G. Pacheco, M.N.D.S. Cordeiro, A. Melo, C. Delerue-Matos, Azithromycin electrochemical detection using a molecularly imprinted polymer prepared on a disposable screen-printed electrode, Anal. Methods 12 (2020) 1486–1494.

[31] T. Zhou, Y. Tao, H. Jin, B. Song, T. Jing, D. Luo, Y. Zhou, Y. Zhou, Y. Lee, S. Mei, Fabrication of a selective and sensitive sensor based on molecularly imprinted polymer/acetylene black for the determination of azithromycin in pharmaceuticals and biological samples, PLoS One 11 (2016), e0147002.

[32] S. Jafari, M. Dehghani, N. Nasirizadeh, M. Azimzadeh, An azithromycin electrochemical sensor based on an aniline MIP film electropolymerized on a gold nano urchins/graphene oxide modified glassy carbon electrode, J. Electroanal. Chem. 829 (2018) 27–34.

[33] O. Vajdle, V. Guzsvány, D. Škorić, J. Csanádi, M. Petković, M. Avramov-Ivić, Z. Kónya, S. Petrović, A. Bobrowski, Voltammetric behavior and determination of the macrolide antibiotics azithromycin, clarithromycin and roxithromycin at a renewable silver – amalgam film electrode, Electrochimica Acta 229 (2017) 334–344.

[34] C. Du, M. Shang, A. Shang, X. Ma, W. Song, Water-soluble VS$_2$ quantum dots with unusual fluorescence for biosensing, Sens. Actuators B Chem. 255 (2018) 926–934.

[35] X. Ma, C. Du, M. Shang, W. Song, VS2 quantum dot label-free fluorescent probe for sensitive and selective detection of ALP, Anal. Bioanal. Chem. 410 (2018) 1417–1426.

[36] H. Sun, et al., Three-dimensional holey-graphene/niobia composite architectures for ultrahigh-rate energy storage, Science 356 (6338) (2017) 599–604.

[37] Z. Wang, H. Guo, R. Gui, H. Jin, J. Xia, F. Zhang, Simultaneous and selective measurement of dopamine and uric acid using glassy carbon electrodes modified with a complex of gold nanoparticles and multiwall carbon nanotubes, Sens. Actuat. B: Chem. 255 (2018) 2069–2077.

[38] H. Jin, H. Guo, X. Gao, R. Gui, Selective and sensitive electrochemical sensing of gastrodin based on nickel foam modified with reduced graphene oxide/silver nanoparticles complex-encapsulated molecularly imprinted polymers, Sens. Actuat. B: Chem. 277 (2018) 14–21.

[39] X. Gao, R. Gui, H. Guo, Z. Wang, Q. Liu, Creatinine-induced specific signal responses and enzymeless ratiometric electrochemical detection based on copper nanoparticles electrodeposited on reduced graphene oxide-based hybrids, Sens. Actuat. B: Chem. 285 (2019) 201–208.

[40] A.M. Mahmoud, M.M. El-Wekil, M.H. Mahnashi, M.F.B. Ali, S.A. Alkahtani, Modification of N, S co-doped graphene quantum dots with p-aminothiophenol-functionalized gold nanoparticles for molecular imprint-based voltammetric determination of the antiviral drug sofosbuvir, Microchim. Acta 186 (2019) 617.

[41] F.A. Mohamed, P.Y. Khashaba, R.Y. Shahin, M.M. El-Wekil, Tunable ternary nanocomposite prepared by electrodeposition for biosensing of centrally acting reversible acetyl cholinesterase inhibitor donepezil hydrochloride in real samples, Colloids Surf. A: Physicochem. Eng. Aspects 567 (2019) 76–85, https://doi.org/10.1016/j.colsurfa.2019.01.033.

[42] J. Feng, X. Sun, C. Wu, L. Peng, C. Lin, S. Hu, J. Yang, Y. Xie, Metallic few-layered VS$_2$ ultrathin nanosheets: high two-dimensional conductivity for in-plane supercapacitors, J. Am. Chem. Soc. 133 (2011) 17832–17838.

[43] D. Gao, Q. Xue, X. Mao, W. Wang, Q. Xu, D. Xue, Ferromagnetism in ultrathin VS$_2$ nanosheets, J. Mater. Chem. C 1 (2013) 5909–5916.

[44] A.V. Murugan, M. Quintin, M. Delville, G. Campet, K. Vijayamohanan, Entrapment of poly (3, 4-ethylenedioxythiophene) between VS$_2$ layers to form a new organic–inorganic intercalative nanocomposite, J. Mater. Chem. 15 (2005) 902–909.

[45] M.M. El-Wekil, A.M. Mahmoud, S.A. Alkahtani, A.A. Marzouk, R. Ali, A facile synthesis of 3D NiFe$_2$O$_4$ nanospheres anchored on a novel ionic liquid modified reduced graphene oxide for electrochemical sensing of ledipasvir: application to human pharmacokinetic study, Biosens. Bioelectron. 109 (2018) 164–170.

[46] S.A. Alkahtani, A.M. Mahmoud, M.H. Mahnashi, R. Ali, M.M. El-Wekil, Facile fabrication of a novel 3D rose like lanthanum doped zirconia decorated reduced graphene oxide nanosheets: an efficient electro-catalyst for electrochemical reduction of futuristic anti-cancer drug salinomycin during pharmacokinetic study, Biosens. Bioelectron. 150 (2020) 111849.

[47] M.M. El-Wekil, S.A. Alkahtani, H.R.H. Ali, A.M. Mahmoud, Advanced sensing nanomaterials based carbon paste electrode for simultaneous electrochemical measurement of esomeprazole and diclofenac sodium in human serum and urine samples, J. Mol. Liq. 262 (2018) 495–503.

[48] F.A. Mohamed, P.Y. Khashaba, R.Y. Shahin, M.M. El-Wekil, A determination approach for rivastigmine by lepidocrocite nanoparticles supported on N-chitosan carbon nanosheets/anti-Fouling PAS: application to biosensing, Electroch. Soc. 166 (2019) H41–H46.

[49] M.H. Mahnashi, A.M. Mahmoud, S.A. Alkahtani, R. Ali, M.M. El-Wekil, Facile fabrication of a novel disposable pencil graphite electrode for simultaneous determination of promising immunosuppressant drugs mycophenolate mofetil and tacrolimus in human biological fluids, Anal. Bioanal. Chem. 412 (2020) 355–364.

[50] E. Mirmomtaz, A.A. Ensafi, H. Karimi-Maleh, Electrocatalytic determination of 6-Thioguanine at a p-aminophenol modified carbon paste electrode, Electroanalysis 20 (2008) 1973–1979.

[51] A.J. Bard, L.R. Faulkner, Electrochemical Methods, Fundamentals and Applications, Wiley, New York, 1980.